

## Numerical study of three-dimensional convection due to buoyancy force in an aluminum oxide melt for Kyropoulos growth

Y. G. Son<sup>a</sup>, J.H. Ryu<sup>a</sup>, W. J. Lee<sup>b</sup>, Y. C. Lee<sup>c</sup>, H. H. Jo<sup>c</sup> and Y. H. Park<sup>a,\*</sup>

<sup>a</sup>Department of Materials Science and Engineering, Pusan National University, 2, Busandaehak-ro 63beon-gil, Geumjeong-gu, Busan 609-735, Korea

<sup>b</sup>Empa Swiss Federal Laboratories for Materials Science and Technology, Überlandstrasse 129, CH-8600 Dübendorf, Switzerland

<sup>c</sup>Dongnam Technology Service Division, Korea Institute of Industrial Technology, 1274 Jisa-dong, Gangseo-gu, Busan 618-230, Korea

Sapphire single crystals are used widely in a number of modern high-tech applications, such as a substrate material for the epitaxial deposition, optical window material and a filter material for thermal neutron beams. In particular, sapphire single crystals have been highlighted for epitaxial gallium nitride films in high-power laser and light emitting diode (LED) industries. Among the many crystal growth methods, the Kyropoulos process is an excellent commercial method for growing larger, high-optical-quality sapphire crystals with fewer defects. Because the properties and growth behavior of sapphire crystals are influenced largely by the temperature distribution and convection of molten sapphire during the manufacturing process, accurate predictions of the thermal fields and melt flow behavior are essential to design and optimize the Kyropoulos crystal growth process. In this study, computational fluid dynamic simulations were performed to examine the effects of the thermal conditions and geometry on melt convection during Kyropoulos sapphire crystal growth. The evolution of various growth parameters on the temperature, pressure, and velocity profiles were examined using three-dimensional, quantitative, finite volume element-based simulations.

**Key words:** Computer simulation, Convection, Radiation, Single crystal growth, Kyropoulos method, Sapphire.

### Introduction

Sapphire (single crystal  $\text{Al}_2\text{O}_3$ ) has excellent mechanical, physical and optical properties, such as high strength, high thermal conductivity and excellent corrosion resistance to acids or strong alkalis compared to other ceramics, such as silica, making it suitable as a material for transmitting windows or domes [1]. Moreover, the low chemical reactivity and appropriate crystal unit parameters make sapphire an excellent substrate in the semiconductor industry for blue light-emitting diodes (LEDs) [2].

A number of methods, such as HEM [3], Kyropoulos (KY) [4] and Czochralski (CZ) [5], have been applied to produce sapphire ingots for commercial applications. Among them, KY is one of the most effective ways of producing single crystal ingots, which enables large sapphire ingots with a diameter of up to 300mm and 65 kg in weight [4]. A KY furnace is typically composed of a crucible located at the center of a furnace, which is surrounded by heating units and slices of cylindrical thermal radiation shields. During KY growth, crystallization occurs with reducing heating

power and by water cooling through a seed load without pulling or rotating. In this method, single crystals are grown directly in the melt by a smooth decrease in temperature at small temperature gradients, which makes it possible to grow crystals with a low dislocation density [6, 7]. The successful growth of sapphire requires good control of heat and mass transport in melt and a crystal because the quality of the grown crystal is closely related to its thermal history and fluid flow behavior in an  $\text{Al}_2\text{O}_3$  melt during the KY process [8].

A computational fluid dynamic (CFD) simulation is one of the methods used to predict the temperature field and flow structure in a KY furnace [9, 10]. Recently Demina *et al.* [4], Chen *et al.* [5] and Lee *et al.* [9] applied numerical analyses successfully to simulate the temperature distribution and flow field in a melt during the KY process. On the other hand, most numerical studies in the literature so far focused on a predictive simulation of sapphire growth for a specific KY system. Therefore, there is little fundamental understanding of the melt convection behavior under different processing conditions.

This study examined the effects of the processing parameters on the melt flow behavior during the KY sapphire growth process. Three dimensional CFD analyses were carried out for KY systems with different aspect ratios and thermal gradients of the melt. In

\*Corresponding author:  
Tel : +82-51-510-2851  
Fax: +82-51-514-4457  
E-mail: yhpark@pusan.ac.kr

addition, the melt flow behavior during the KY process as well as pressure fields inside the melt were investigated in terms of the crucible geometry and applied thermal conditions.

## Numerical Modeling

A KY sapphire growth system with a  $6.28 \times 10^{-3} \text{ m}^3$  cylindrical crucible, in which a cylindrical seed was located at the center of the free surface of the melt, was considered. Fig. 1 shows a schematic diagram, geometry and meshes of CFD models used for the analyses. To simplify the simulations, the physical properties of the melt and crystal were assumed to be isotropic. Table.1 lists the physical properties of the sapphire and melt used in this study. In the model, the melt was assumed

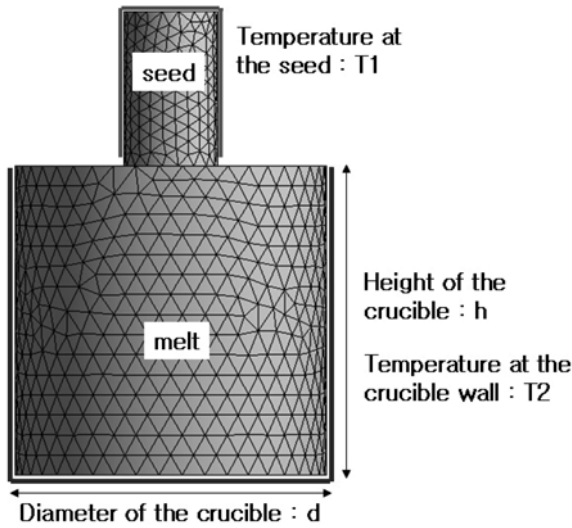


**Fig. 1.** schematic diagram of the crucible geometry in the Kyropoulos growth system for 3D modeling.

**Table.1** physical properties of the aluminum oxide used in this study.

Properties	Values
Thermal conductivity of the crystal (kc, W/m K)	5
Thermal conductivity of the melt (km, W/m K)	2.05
Specific heat (Cp, J/kg K)	1430
Density ( $\rho$ , kg/m <sup>3</sup> )	3970
Latent heat of solidification ( $\Delta H$ , J/kg)	1,407,000
Melting temperature (Tm, K)	2327
Dynamic viscosity ( $\mu$ , kg/m S)	0.057
Thermal expansion coefficient ( $\beta$ , K <sup>-1</sup> )	1.8x10-5
Transparent band ( $\mu\text{m}$ )	0.5 ~ 4.5
Absorption coefficient ( $\tilde{K}$ , m <sup>-1</sup> )	19.26
Scattering coefficient ( $\sigma$ )	0
Refractive index ( $\eta$ )	1.78

to be a viscous and incompressible Newtonian fluid with a Boussinesq approximation. Each model was meshed with tetrahedral elements through the automatic meshing algorithm package of Fluent [11]. Before performing the main calculations, the grid independence of the numerical results was examined with a different grid size. Approximately 20,000 elements with a mean grid size of 15 mm were found to be fine enough to reach a grid independent solution.

The governing equations used for the dynamics of the melt flow employed basic Navier-Stokes equations. The temperature distribution in the melt and crystal depends largely on radiation because both the melt and crystal are semi-transparent. In this study, the Discrete Ordinates radiation (DO) model [12] was used for heat transfer by radiation. The DO model solves the radiative transfer equation for a finite number of solid angles, each associated with a vector direction  $\vec{S}$  fixed in the global Cartesian system (x,y,z). The  $4\pi$  angular space at any spatial location was discretized into  $10 \times 10$  solid angles. The equation can be written as follows:

$$\begin{aligned} & \nabla \cdot (I_{\lambda}(\vec{r}, \vec{S}) \cdot \vec{S}) + (\tilde{k} + \sigma_s) \cdot I_{\lambda}(\vec{r}, \vec{S}) \\ & = \tilde{k} \cdot n^2 \cdot I_{b\lambda} + \frac{\sigma_s}{4\pi} \cdot \int_0^{4\pi} I_{\lambda}(\vec{r}, \vec{S}') \Phi(\vec{S}, \vec{S}') d\Omega' \end{aligned}$$

where  $I$  is the radiation intensity, which depends on the position  $\vec{r}$  and direction  $\vec{S}$ ,  $\tilde{k}$  is the absorption coefficient,  $\sigma_s$  is the scattering coefficient,  $n$  is the refractive index,  $\Phi$  is the phase function,  $\Omega'$  is the solid angle and  $I_{b\lambda}$  is the black body intensity given by the Planck function.

The numerical problems were implemented using the commercial finite volume program, Fluent, with three dimensional double precision, second order upwind discretization for convection, SIMPLE (Semi-Implicit Method for Pressure-Linked Equations) algorithm for pressure-velocity coupling and the PRESTO (PREssure STaggering Option) scheme for pressure interpolation.

## Results

### Effects of thermal condition

In this section, the effects of the thermal condition were observed. To investigate the effects of thermal condition, the temperatures of the crucible wall ( $T_2$ ) chosen were 2329K, 2331K, 2333K and 2335K with an aspect ratio of 1.0, and the temperature of the seed ( $T_1$ ) was fixed at 2323K. For the thermal condition, the Grashof number ( $Gr$ ),  $Gr = \rho \cdot \beta \cdot g \cdot L^3 \cdot \Delta T / \mu$ , was varied. In natural convection, the basic driving force is buoyancy, which is caused by density differences in the fluid due to a temperature gradient. Therefore, it is possible to compare the intensities of natural convection between models with a different  $T_2$  during sapphire crystal growth by calculating the  $Gr$  number,

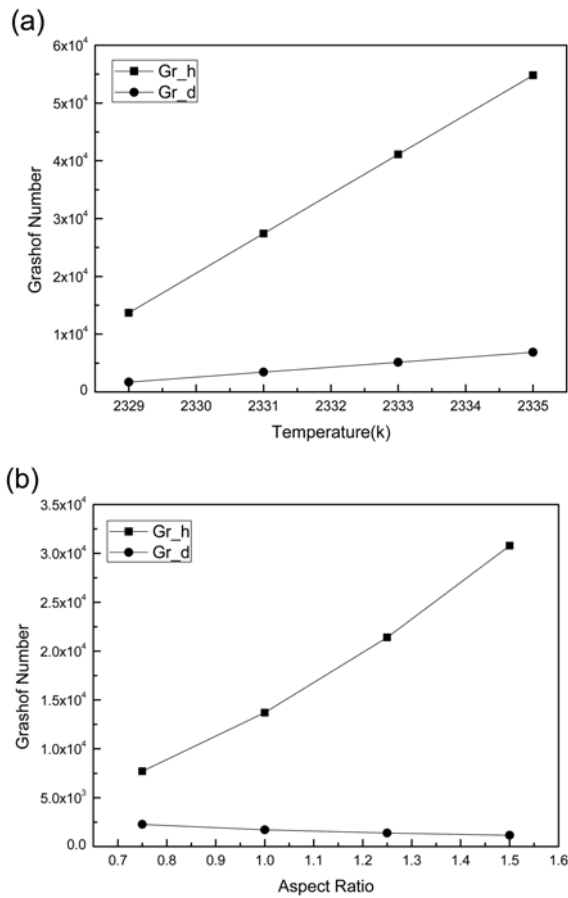


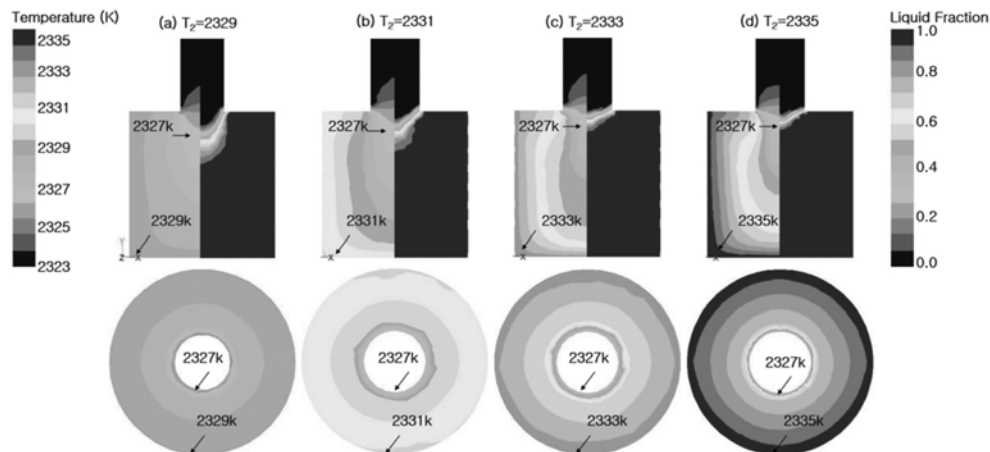
**Fig. 2.** Grashof Number calculated in the vertical direction and horizontal direction versus (a) thermal condition ( $T_2$ ) and (b) aspect ratio of the crucible geometry.

which is a function of temperature. Fluid flow for natural convection from a vertical plate typically tends to transit from laminar to turbulent above a Gr number of  $10^8$ . The Gr numbers calculated for the different thermal condition ( $T_2$ ) models were  $1.37E + 04$ ,  $2.74E + 04$ ,  $4.11E + 04$  and  $5.4E + 04$  in the vertical direction and  $1.71E + 03$ ,  $3.42E + 03$ ,  $5.13E + 03$  and

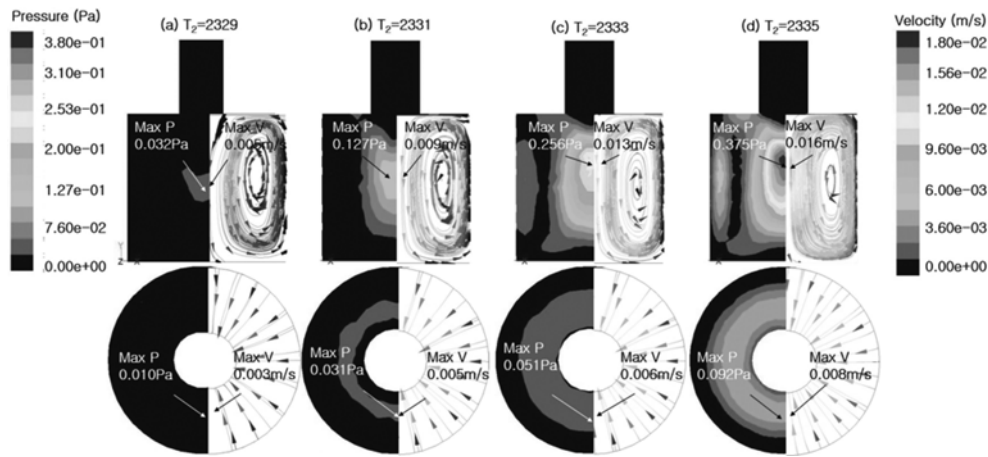
$6.85E + 03$  in the horizontal direction (Fig. 2(a)), corresponding to each of the crucible wall temperatures ( $T_2$ ). The Gr numbers in both directions increased linearly with increasing  $T_2$ . The increase rate of the Gr number in the vertical direction was higher than that in the horizontal direction. Since higher Gr numbers in both directions suggest a larger driving force for fluid flow, natural convection inside the sapphire melt becomes stronger and faster as  $T_2$  is increased.

Fig. 3 shows the isotherms (left) with the liquid fractions (right) for models with different crucible wall temperatures ( $T_2$ ). The liquid fraction was approximately 0.9 of the initial state during the crystallization process. The shapes of the isotherms between models were almost identical despite the temperature gradients increasing in both the vertical and horizontal directions. From the top view, the isotherms of the models formed concentric circular shapes and the temperature gradients increased linearly. The melt flow rose up near the wall and moved down in the center because the temperature near the side wall and bottom was higher than inside the melt. Heat transfer in the melt is governed mainly by these buoyancy convections due to the relatively high Prandtl number ( $Pr = \mu/C_p \cdot \rho = 40$ ).

The intensity and shape of the melt flow were examined by observing the maximum dynamic pressure field (left) and velocity streamline (right) (Fig. 4). The dynamic pressure is closely related to the kinetic energy of melt convection. The maximum dynamic pressure was observed at the center inside the melt because the fluid streams were concentrated at the center from all outside directions. In addition, its intensity became stronger linearly with increasing  $T_2$ . Looking into the top view, the maximum dynamic pressure on the free surface also increased linearly. In addition, the maximum velocity was found at the center of the crucible and the rate of the melt flow at the center and on the free surface became faster linearly with increasing buoyancy force as  $T_2$  was increased, as



**Fig. 3.** Instantaneous isotherms (left) and liquid fraction (right) for the aspect ratio of the crucible geometry  $h/d = 1$ , thermal condition (a)  $T_2 = 2329$ , (b)  $T_2 = 2331$ , (c)  $T_2 = 2333$ , (d)  $T_2 = 2335$ .



**Fig. 4.** Instantaneous isobars of dynamic pressure (left) and velocity streamline (right) for the aspect ratio of the crucible geometry  $h/d = 1$ , thermal condition (a)  $T_2 = 2329$ , (b)  $T_2 = 2331$ , (c)  $T_2 = 2333$ , (d)  $T_2 = 2335$ .

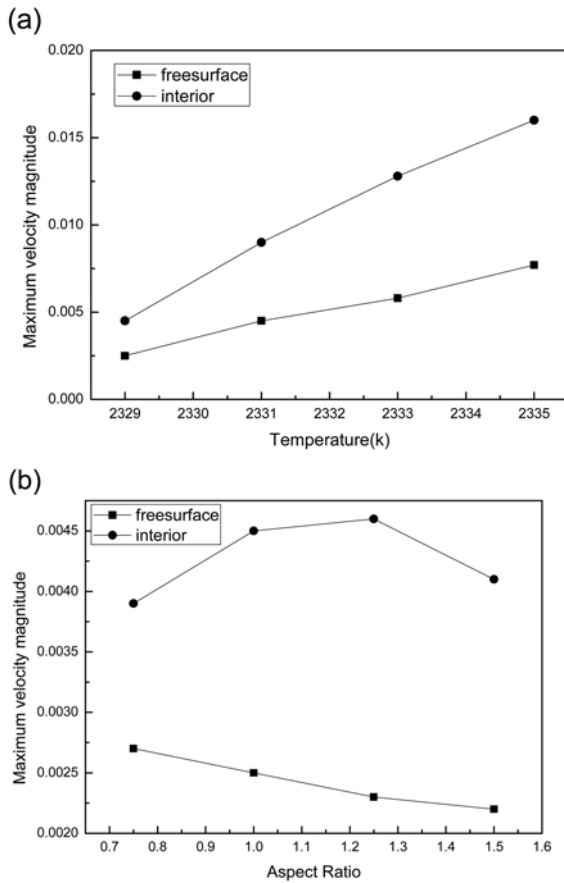


**Fig. 5.** Maximum velocity magnitude inside the melt and on the free surface versus (a) thermal condition ( $T_2$ ) and (b) aspect ratio of the crucible geometry.

shown in Fig. 5(a). The shape of melt flow was composed of a single large vortex, which was similar regardless of its thermal condition because melt flow motion depends strongly on the geometry of the crucible. The results showed that the maximum velocity and maximum dynamic pressure were directly in proportion to the Gr number and  $T_2$ .

During growth, crystals are subjected to stresses that arise mainly from thermal factors. In oxide crystal growth, it is particularly important to control the defects produced by these stresses because of the close relationship between crystalline and optical perfection [13]. Precise control of the thermal conditions is required to lower the thermal stress by reducing the driving force for melt convection.

#### Analysis of the effects of aspect ratio

In this section, the effects of geometry of the crucible were observed. To examine the effects of the geometry, four models were designed with different aspect ratios,  $h/d = 0.75$ ,  $h/d = 1.0$ ,  $h/d = 1.25$  and  $h/d = 1.5$ , which have the same volume ( $6.28 \times 10^{-3} \text{ m}^3$ ) and crucible wall temperature ( $T_2 = 2329\text{K}$ ). The Gr numbers were calculated in the vertical direction ( $7.69\text{E} + 03$ ,  $1.37\text{E} + 04$ ,  $2.14\text{E} + 04$  and  $3.08\text{E} + 04$ ) and horizontal direction ( $2.28\text{E} + 03$ ,  $1.71\text{E} + 03$ ,  $1.38\text{E} + 03$  and  $1.15\text{E} + 03$ ), corresponding to each of its geometries (in Fig. 2(b)). The Gr number increased approximately three times in the vertical direction when the aspect ratio of the crucible geometry was increased from 0.75 to 1.5, whereas it decreased slightly in the horizontal direction. This is because the Gr number is a function of distance, which is proportional to the cube of  $L^3$ . This means that the driving force of melt convection tends to become stronger in the vertical direction while diminishing in the horizontal direction.

Fig. 6 presents isotherms (left) and liquid fractions (right) of the models with different aspect ratios. The liquid fraction for all models was approximately 0.9. The isotherms elongated in the vertical direction with increasing aspect ratio of the crucible geometry. On the free surface, shapes of the isotherms were almost circular. The temperature on the free surface was the highest near the crucible wall and the lowest near the seed, as expected. Fig. 7 shows the dynamic pressure field (left) and velocity streamline (right) of the models

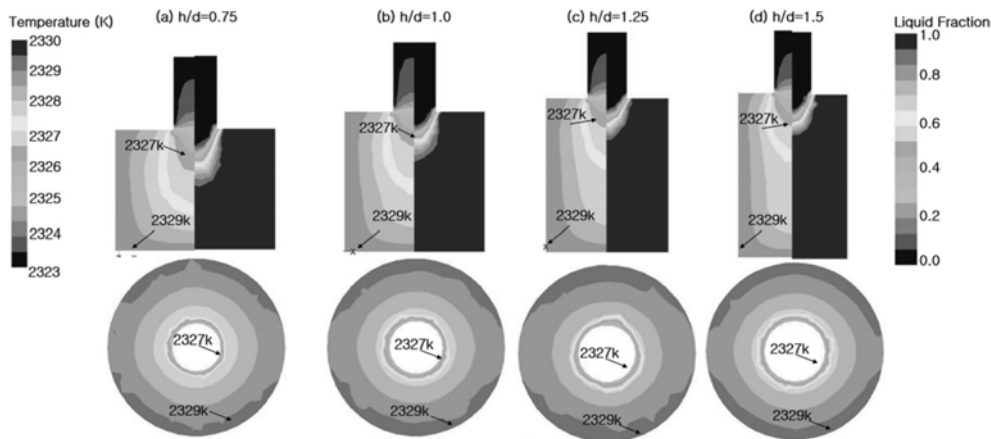


**Fig. 6.** Instantaneous isotherms (left) and liquid fraction (right) for thermal condition  $T_2 = 2329$ , aspect ratio of the crucible geometry (a)  $h/d = 0.75$ , (b)  $h/d = 1.0$ , (c)  $h/d = 1.25$ , (d)  $h/d = 1.5$ .

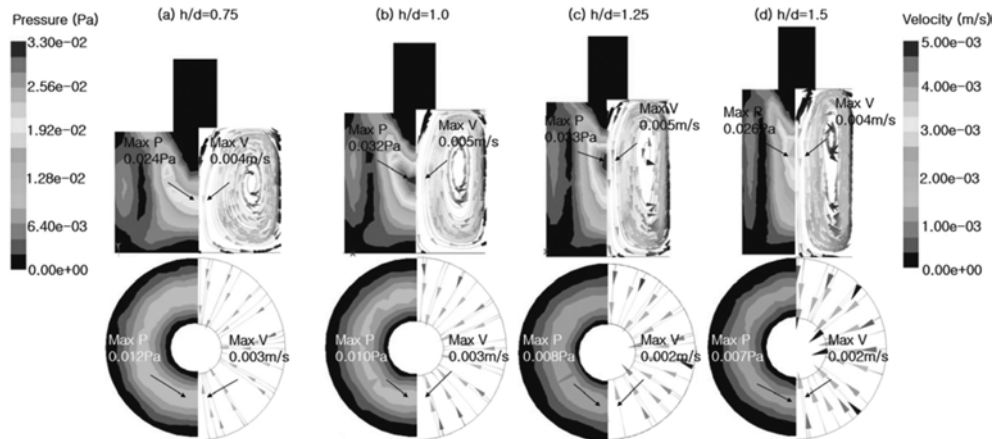


**Fig. 7.** Instantaneous isobars of the dynamic pressure(left) and velocity streamline(right) for the thermal condition  $T_2 = 2329$ , aspect ratio of the crucible geometry (a)  $h/d = 0.75$ , (b)  $h/d = 1.0$ , (c)  $h/d = 1.25$ , (d)  $h/d = 1.5$ .

with different aspect ratios. The isobars and velocity streamline of the melt were transformed to perpendicular from transverse with the center of the vortex moving up as the aspect ratio was increased. The distribution and intensity of the maximum dynamic pressure and the maximum velocity on the free surface were similar regardless of the aspect ratio of the crucible geometry. In Fig. 5 (b), the maximum velocity inside the melt increased with increasing aspect ratio until 1.25 and decreased at higher aspect ratios. The aspect ratio of the geometry between 1.0 and 1.25 is more effective in melt convection, which makes the melt flow faster and stronger inside the melt. In natural convection for a rectangular enclosure, the aspect ratio has a strong impact on the flow patterns [14]. A small aspect ratio leads to decrease the effect of the buoyancy force and a large aspect ratio enhances the shear stress effect. Overall, an aspect ratio  $< 1.0$  should produce a high quality sapphire crystal considering the lower Gr number and melt flow rate for a lower dislocation density with weaker buoyancy convection.

## Conclusions

CFD analyses for KY systems were carried out successfully using three dimensional modeling to examine the effect of the processing parameters on the melt flow behavior during KY sapphire growth process. The melt flow structures were not changed significantly with changing Gr and  $T_2$ , while the maximum dynamic pressure was directly proportional to Gr and  $T_2$ . As a result, the melt flow velocity became faster gradually due to the higher buoyancy force with increasing  $T_2$ , which might affect the quality of as-grown crystal significantly. Therefore, the thermal conditions should be controlled carefully to maintain a slower rate of melt flow.

The flow pattern of the sapphire melt was influenced by the crucible geometry. With a higher aspect ratio of the crucible, the shape of the vortex inside the melt changed from a circular one to an elongated one in the vertical direction. In addition, the center of the vortex inside the melt moved up as the aspect ratio was increased. The maximum dynamic pressure and the

maximum velocity inside the melt were highest at an aspect ratio of 1.25. The Gr number increased approximately three times in the vertical direction when the aspect ratio of the crucible geometry was increased from 0.75 to 1.5, whereas it decreased slightly in the horizontal direction. Overall, an aspect ratio  $< 1.0$  is suitable for a stable flow pattern with a lower Gr number and lower flow rate of the melt.

### Acknowledgments

This work was supported by a 2-Year Research Grant of Pusan National University.

### References

1. A. Wang, G. Pickrell, R. May, Single-Crystal Sapphire Optical Fiber Sensor Instrumentation, Virginia Polytechnic Institute (US) Technical Report Chap. 3 (2002).
2. Daniel C. Harris, A Century of Sapphire Crystal Growth, Proceedings of the 10th DoD Electromagnetic Windows Symposium, Norfolk, Virginia, May 2004.
3. Chandra P. Khattak, Frederick Schmid, Growth of the world's largest sapphire crystals, *Journal of Crystal Growth* 225 (2001) 572-579.
4. S.E. Demina, E.N. Bystrova, M.A. Lukanina, V.M. Mamedov, V.S. Yuferev, E.V. Eskov, M.V. Nikolenko, V.S. Postolov, V.V. Kalaev, Numerical analysis of sapphire crystal growth by the Kyropoulos technique, *Optical Materials* 30 (2007) 62-65.
5. Chung-Wei Lu, Jyh-Chen Chen, Chien-Hung Chen, Chun-Hung Chen, Wen-Ching Hsu, Che-Ming Liu, Effects of RF coil position on the transport processes during the stages of sapphire Czochralski crystal growth, *Journal of Crystal Growth* 312 (2010) 1074-1079.
6. Chun-Hung Chen, Jyh-Chen Chen, Chung-Wei Lu, Che-Ming Liu, Numerical simulation of heat and fluid flows for sapphire single crystal growth by the Kyropoulos method, *Journal of Crystal Growth* 318 (2011) 162-167.
7. <http://iscrystals.com>, Institute for Single Crystals, National Academy of Sciences of Ukraine.
8. S.E. Demina, V.V. Kalaev, 3D unsteady computer modeling of industrial scale Ky and Cz sapphire crystal growth, *Journal of Crystal Growth* 320 (2011) 23-27.
9. W.J. Lee, Y.C. Lee, H.H. Jo, Y.H. Park, Effect of crucible geometry on melt convection and interface shape during Kyropoulos growth of sapphire single crystal, *Journal of Crystal Growth* 324 (2011) 248-254.
10. A.T. Kuliev, N.V. Durnev, V.V. Kalae, Analysis of 3D unsteady melt flow and crystallization front geometry during a casting process for silicon solar cells, *Journal of Crystal Growth* 303 (2007) 236-240.
11. Fluent Inc., *Fluent 12.0 User's Guide*, Pennsylvania: Canonsburg, 2009.
12. Fluent Inc., *Fluent 12.0 Theory Guide*, Pennsylvania: Canonsburg, 2009.
13. B. Cockayne, Developments in melt-grown oxide crystals, *Journal of Crystal Growth* 3, 4 (1968) 60-70.
14. Wei Tong, Aspect ratio effect on natural convection in water near its density maximum temperature, *International Journal of Heat and Fluid Flow* 20 (1999) 624-633.